



AIAA 2001-0369

Thermal Analysis of a High-Speed
Aircraft Wing Using p -Version Finite
Elements

Dana C. Gould
NASA Langley
Hampton, VA

**39th AIAA Aerospace Sciences
Meeting & Exhibit**
8-11 January 2001 / Reno, NV

For permission to copy or to republish, contact the American Institute of Aeronautics and Astronautics,
1801 Alexander Bell Drive, Suite 500, Reston, VA, 20191-4344.

THERMAL ANALYSIS OF A HIGH-SPEED AIRCRAFT WING USING p -VERSION FINITE ELEMENTS

Dana C. Gould

NASA Langley Research Center
Hampton, Virginia 23681-2199

ABSTRACT

This paper presents the results of conceptual level thermal analyses of a High Speed Civil Transport (HSCT) wing using p -version finite elements. The work was motivated by a thermal analysis of a HSCT wing structure which showed the importance of radiation heat transfer throughout the structure. The analysis also showed that refining a traditional finite element mesh to accurately capture the temperature distribution on the internal structure led to very large meshes with unacceptably long execution times. Further study indicated using p -version finite elements might improve computation performance for this class of problem. Methods for determining internal radiation heat transfer were then developed and demonstrated on test problems representative of the geometry found in an aircraft wing structure.

This paper presents the results of the application of these new methods to the analysis of a high speed aircraft wing. Results for both a wing box model as well as a full wing model are presented. The reduced wing box model allows for a comparison of the traditional finite element method with mesh refinement (h -refinement) to the new p -version finite elements while the full wing model demonstrates the applicability and efficiency of p -version finite elements for large models.

INTRODUCTION

This effort began with a study of the thermal analysis of a high-speed civilian transport vehicle wing to determine the current state of thermal analysis capabilities for such a problem. That study, which used commercially available thermal analysis software, is

documented in an earlier paper.¹ The primary difficulty in the analysis was accurately modeling the radiation heat transfer internal to the wing structure. Initial analyses using a coarse mesh and including conduction and radiation heat transfer were run successfully; however, the large element size produced inaccurate temperatures for the internal structure. To improve the results, the analysis was repeated using a refined mesh. The initial run of the refined model considered heat transfer throughout the wing by conduction only, and produced a solution with reasonable temperature distributions on the internal structure. Internal radiation exchange was then added to the model, but the solution of the model never successfully completed.

To get temperature predictions for the internal structure, including the effects of internal radiation heat transfer, a reduced model was generated. The reduced model included a single wing-box section of the wing. This model was run both with and without internal radiation exchange, and the results showed that internal radiation exchange had a significant effect on the temperatures of the internal structure.

Thus a method that could analyze a full wing with internal radiation was desired, and the application of the p -method appeared promising based on the work in reference 1. This paper presents the results of applying the methods developed in reference 1 to the thermal analysis of a High Speed Civil Transport (HSCT) wing.

WING-BOX MODEL

Before analyzing the full wing, a model of a single wing-box was developed. The term wing-box refers to the open area enclosed by adjacent ribs and spars and the corresponding upper and lower surface sections of a wing. The ribs and spars make up the internal structure

Copyright © 2001 by the American Institute of Aeronautics and Astronautics, Inc. No copyright is asserted in the United States under Title 17, U.S. Code. The U.S. Government has a royalty-free license to exercise all rights under the copyright claimed herein for Governmental purposes. All other rights are reserved by the copyright owner.

of the wing with the spars running from the fuselage to the wing tip, and the ribs running from the leading edge of the wing to the trailing edge of the wing. The ribs and spars of the full wing model are shown in Figure 1. The wing-box model was developed so that results from the new p -element methods could be compared with the results obtained from traditional methods.

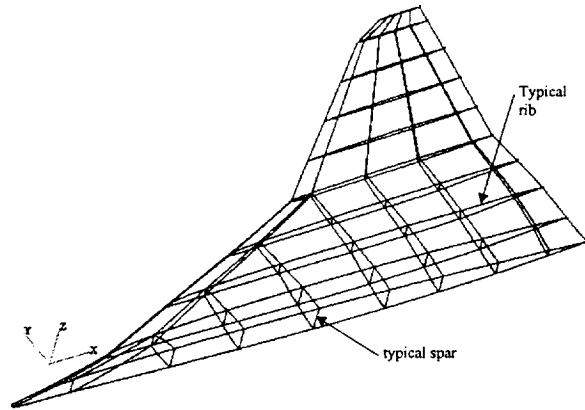


Figure 1: High Speed Civil Transport wing geometry including skin, ribs, and spars.

The wing-box, shown in Figure 2, is 60 inches long (fore to aft) by 15 inches wide (port to starboard) by 30 inches high (thickness of wing). The vertical surfaces of the wing-box represent the internal structure (ribs and spars) and are adiabatic on their external faces. The upper and lower surfaces of the wing-box represent the upper and lower surfaces of the wing skin and are subjected to convective heating due to the airflow over the wing. The convection boundary conditions on the upper and lower surface were taken from a mid-wing location of the full wing model described in the following sections. The methods used to generate the convection boundary conditions are discussed in the following section as well. Convective heating was applied to the upper and lower surfaces of the wing-box assuming uniform flow over the surfaces. The convection coefficients for both the upper and lower surfaces are given in Table 1 and are assumed to remain constant throughout the trajectory. Since there is little difference in the recovery temperatures for the upper and lower surfaces, the same time-dependent values were used for both and are listed in Table 2. Heat transfer due to natural convection internal to the wing-box was ignored.

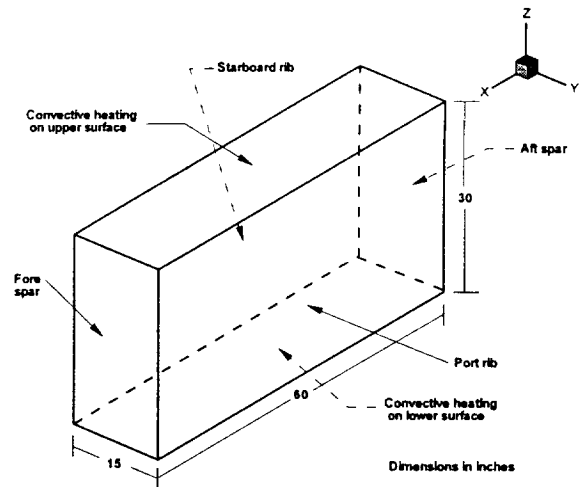


Figure 2: Geometry of wing-box model.

Table 1: Convection coefficients for wing-box model.

Surface	Convection Coefficient BTU/hr-in ² -°F
Upper	0.06
Lower	0.84

Table 2: Convection recovery temperatures for wing-box model.

Time (hours)	Fluid Temperature (°F)
0.00	59
0.20	334
4.37	336
5.00	61

The six surfaces forming the wing-box use a corrugated panel construction as shown in Figure 3. The panels are made from titanium and the thermal properties for this material are listed in Table 3. The corrugated panels are modeled with isotropic elements with an equivalent thickness of 0.065 inches. This thickness represents the thickness of the face sheet (0.015 inches) plus the thickness of the core sheet (0.05 inches). All of the internal faces of the wing-box radiate to each other as diffuse-gray surfaces, and the upper and lower skin surfaces also radiate to space. All

surfaces have an emissivity of 0.85, and the upper surface has an absorbed heat flux of 1.5 BTU/hr-in² due to solar heating. The lower surface has a combined solar and earth IR heating of 0.89 BTU/hr-in².



Figure 3: Corrugated panel construction.

Table 3: Thermal properties used in wing-box model.

Material	Titanium
Density	0.16(lb/in ³)
Specific heat	0.135(BTU/lb-°F)
thermal conductivity	0.343(BTU/hr-inch-°F)

Analysis with p -refinement

The wing-box was analyzed using the new p -element methods with a single element for each of the six surfaces of the wing-box. Cases were run with p values ranging from 1 to 6. Results were obtained for both the radiation sub element and integration methods (see reference 1). Each analysis was run using a time step of 0.1, 0.05, and 0.01 hours with temperature results output at every time step. Results for the different time steps were similar and the results presented here are from the runs using a 0.05 hour time step. Figure 4 shows temperature contours at time = 0.3 hours for the case of $p=1$ using the radiation sub-element method and Figure 5 shows the same case with $p=2$ elements. For $p=1$, the radiation sub-element approach reverts to the traditional methods similar to those employed in commercial finite element heat transfer software. Comparing the contours for the $p=1$ case to the $p=2$ case, significant differences can be seen because the $p=1$ mesh does not adequately model the side walls of the wing-box. For the $p=1$ case, the nodes for the side wall elements are located on upper and lower surfaces with no nodes in-between. With no nodes between the upper and lower surfaces, the temperature of the sidewalls cannot be computed accurately. The nodes on the upper and lower surfaces are shared by the upper and lower surface elements which have the convection

boundary conditions. The convection boundary conditions drive the temperatures of these nodes and the temperature lag midway between the upper and lower surfaces is not captured.

Figure 6 shows temperature contours for the integration method case with $p=4$ elements, at 0.3 hours after takeoff. The results are similar to the $p=2$ results in Figure 5, with the temperatures in the middle of the vertical surfaces (the internal structure) slightly warmer. In fact, the results do not change significantly for higher-order elements. Figure 7 shows the results for the integration method using $p=6$ elements. In the cases run here, the results for the radiation sub element method and the integration method were similar.

To see the transient nature of the temperatures gradients in the wing-box, two temperatures from the forward rib-port spar junction have been plotted versus time. Point A is at the intersection of the fore spar, the port rib, and the lower surface while point B is along the spar-rib edge halfway between the upper and lower surfaces (see Figure 7). Figure 8 shows the temperature histories computed using the radiation sub-element method with $p=2$ elements, and Figure 9 shows the results from the integration method using the $p=6$ results. Figure 8 shows that point B initially drops in temperature with the $p=2$ elements. This behavior is a consequence of using a consistent mass matrix in the transient solution algorithm in a problem with rapid temperature change (see, for example, p. 334 of [2]). The temperature drop had the same approximate magnitude and duration regardless of the time step used (0.1 hours, 0.05 hours, 0.01 hours). Switching to a backwards difference for the time derivative eliminated the temperature drop; however, the backwards difference is only first-order accurate whereas the central difference used in the Crank-Nicholson method is second-order accurate. Note however, that the temperature drop did not occur for the higher-order elements as shown Figure 9 for the $p=6$ elements. Lobo and Emery [3] studied this behavior and concluded that the higher-order elements are not immune from this anomalous behavior but simply less susceptible to it.

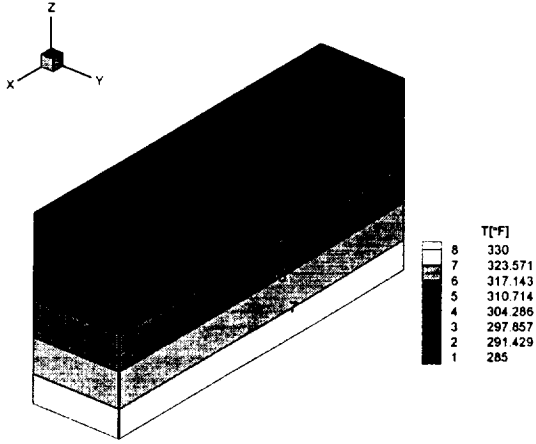


Figure 4: Temperature contours of the wing-box model using the radiation sub element method with $p=1$ elements at 0.3 hours.

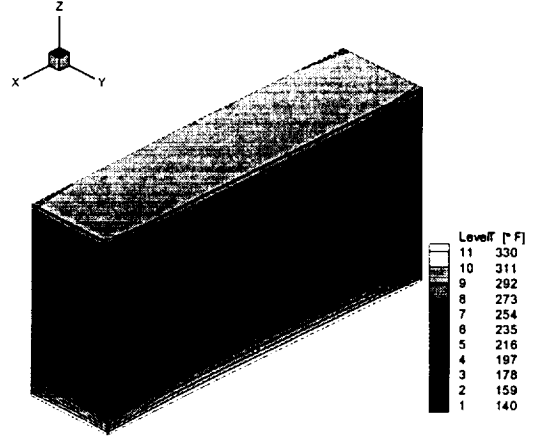


Figure 6: Temperature contours of the wing-box model using the integration method with $p=4$ elements at 0.3 hours.

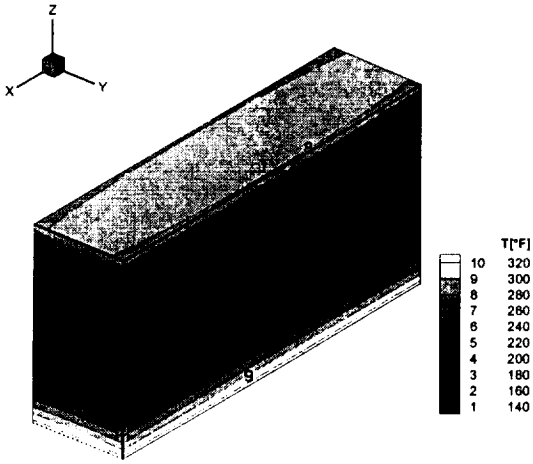


Figure 5: Temperature contours of the wing-box model using the radiation sub-element method with $p=2$ elements at 0.3 hours.

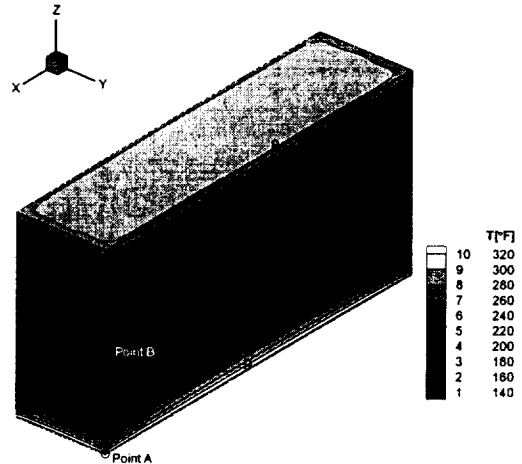


Figure 7: Temperature contours of the wing-box model using the integration method with $p=6$ elements at 0.3 hours.

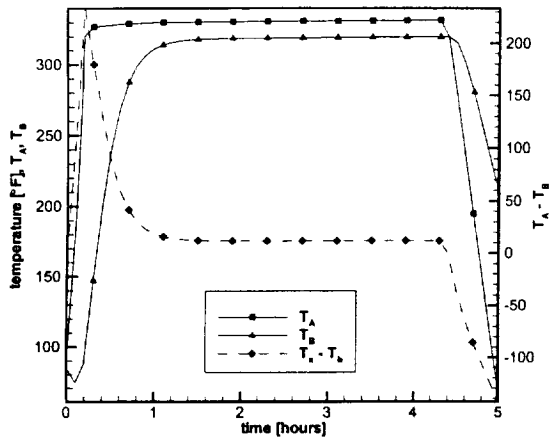


Figure 8: Transient temperature response at selected points of the wing-box model using the radiation sub-element method with $p=2$ elements. (Location of points shown in Figure 7.)

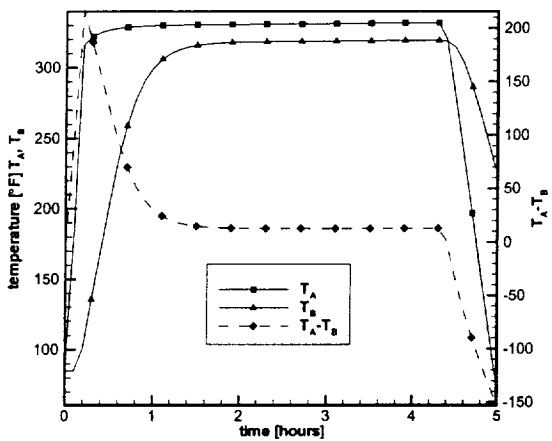


Figure 9: Transient temperature response at selected points of the wing-box model using the integration method with $p=6$ elements. (Location of points shown in Figure 7.)

Analysis with h -refinement

Several finite element analyses were made of the wing-box using the traditional radiation methods with h -refinement. In these analyses, each surface was subdivided into an n by n mesh where n varied from 1 to 10 (the view factor code was the limiting factor in increasing the mesh size). Results for the 2 by 2, 5 by 5, and 10 by 10 meshes are shown in Figure 10-12. The h -refinement behavior shown in these figures is similar to the behavior seen in the p -enrichment cases, but note that the lowest order p results ($p=2$) are similar to the results from the largest n by n mesh case.

The traditional method does however have one advantage, speed. Table 4 lists the number of degrees of freedom and the execution time for several cases. The execution times were obtained on a 133 MHz Pentium PC with 32 Mbytes of RAM. For a given number of degrees of freedom the traditional method is faster than the radiation sub-element method which in turn is faster than the integration method. The differences in run times increase significantly as the element order increases in the p -method. However, a comparison based on the degrees of freedom does not account for the improved accuracy of the higher-order methods. The contour plots show the $p=2$ solution to be the most similar to the traditional method with a 10 by 10 mesh (the most refined mesh used) but with a significantly lower execution time. This result is consistent with the results in reference [1] where a more rigorous accuracy comparison of the methods was presented.

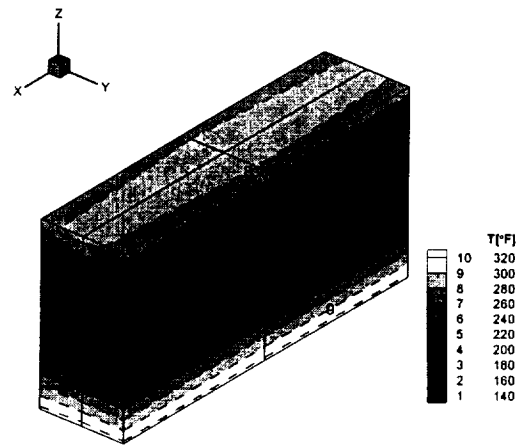


Figure 10: Temperature contours for wing-box model case 12 (2 elements per edge or 4 elements per surface) at 0.3 hours.

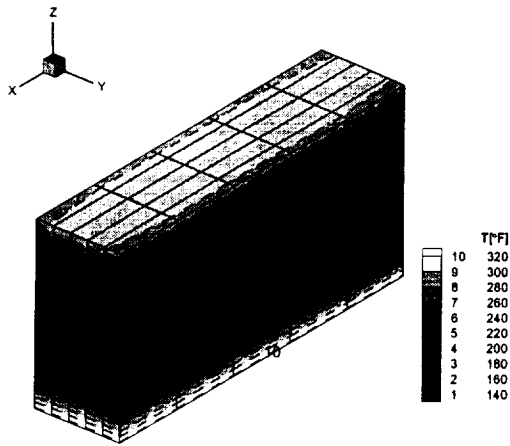


Figure 11: Temperature contours for wing-box model case 14 (5 elements per edge, 25 elements per surface) at 0.3 hours.

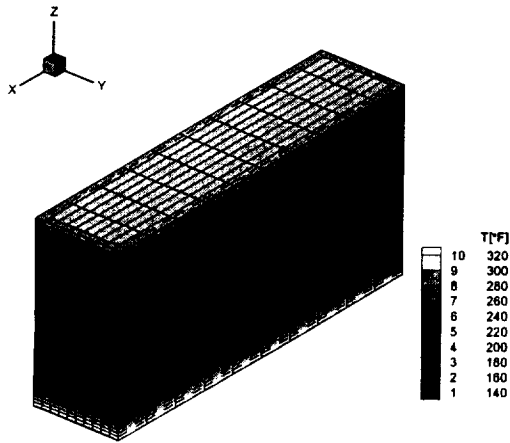


Figure 12: Temperature contours for wing-box model case 15 (10 elements per edge, 100 elements per surface) at 0.3 hours.

Table 4: Execution times for wing-box model using new methods versus traditional methods.

Case	Method*	element p	elements per edge (n)	# of DOF	Execution time (sec.)
1	RSE	2	1	26	72
2	RSE	3	1	56	193
3	RSE	4	1	98	502
4	RSE	5	1	152	1261
5	RSE	6	1	218	2733
6	IM	2	1	26	315
7	IM	3	1	56	996
8	IM	4	1	98	2867
9	IM	5	1	152	6777
10	IM	6	1	218	16200
11	TM	1	1	8	9.1
12	TM	1	2	26	37
13	TM	1	3	56	84
14	TM	1	5	152	360
15	TM	1	10	602	17018

*RSE = Radiation sub-element method, IM = Integration method, TM = Traditional Method

FULL WING ANALYSIS

Description

The next analysis is of a complete HSCT wing. The analysis presented here is typical of a conceptual level design effort that integrates several disciplines to evaluate the feasibility of a proposed vehicle. The system analysis begins with an aerodynamic analysis of the proposed vehicle at selected points throughout the trajectory. Aerodynamic heating data is then used in a thermal analysis of the vehicle to predict temperatures throughout the structure. These temperatures are then transferred to a structural model of the vehicle along with the pressure loads from the aerodynamic analysis. The structural model is used to size the load-carrying components of the vehicle, typically through an optimization process. The final component sizing determines component level and overall vehicle weight. The weight data, trajectory data, and aerodynamic data are then used in a trajectory analysis to determine the overall viability of the vehicle. The entire process is then iterated until a final optimized design is determined.

The conceptual level design used in this process produces thermal and structural models with simple geometric elements. For example, holes that commonly occur in the internal structure of the wing are not considered at this stage, but are left to the detailed design process. The goal of the thermal and structural analyses in this process is not to analyze a

particular design in great detail, but rather to accurately evaluate multiple conceptual designs in order to arrive at an optimum structure.

The thermal analysis of an entire vehicle is often performed using individual models for the major components of the vehicle. The analysis presented here is of a wing structure of a high-speed civil transport. The geometry used in the analysis was supplied by the GEOLAB group at NASA Langley Research Center. The wing, shown in Figure 1, is approximately 113 feet long at the root, and 55 feet wide at the trailing edge. The structure consists of the upper and lower skin surfaces of the wing as well as the internal structure of ribs and spars. The skin surfaces represent the outer mold line of the wing and are consistent with the geometry used for aerodynamic analysis.

The wing skin uses the same corrugated panel construction used in the wing-box model, which is shown in Figure 3. The panels were modeled using the same material properties used for the wing-box model which are listed in Table 3. As in the wing-box model, the corrugated panels are modeled with isotropic elements with an equivalent thickness of 0.065 inches. This thickness represents the thickness of the face sheet (0.015 inches) plus the thickness of the core sheet (0.05 inches). For simplicity, the internal structure was assumed to be made of the same corrugated panel construction.

Aerodynamic Heating

A five-hour flight trajectory representative of a commercial airline or transport route was used in the analysis. The Mach 2.4 cruise lasts 3.8 hours and reaches a maximum altitude of 70,000 feet. Figure 13 shows the altitude and speed of the vehicle throughout the trajectory, the analysis does not include any special maneuvers (for example an emergency descent) which often drive the design of an aircraft.

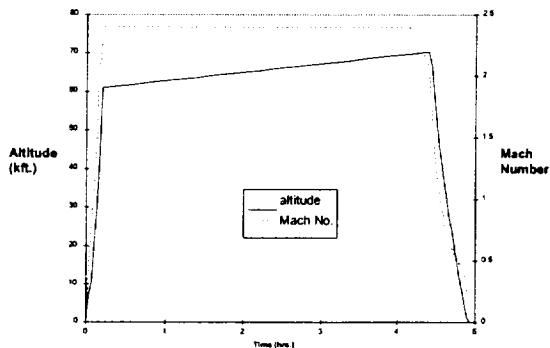


Figure 13: Mach number and altitude for commercial route of a High Speed Civil Transport.

To compute the convection boundary conditions over the full wing, NASA Langley's version of the MINIVER computer code, LANMIN [4], was used. The upper and lower surfaces were subdivided to give one surface element between adjacent pairs of ribs and spars. The surface elements of Figure 1 represent the surface elements used to compute the convection boundary conditions. The centroid of each surface was computed along with the distance from the leading edge of the wing to the surface centroid. This data was then combined with the trajectory data to compute a convection coefficient and recovery temperature for every surface element in Figure 1 at every trajectory point. Upon inspection of the data, and based on results of some wing-box model runs, it was determined that the convection boundary condition could be accurately modeled using only four trajectory points and interpolating the data between points. This greatly reduced the amount of data that had to be transferred to the finite element model without a significant loss in accuracy.

Full Wing Finite Element Thermal Model

The full wing model was meshed using one element to represent each surface shown in Figure 1. Thus the mesh used in the aerodynamic heating analysis is coincident with the thermal analysis mesh and each wing surface element has a separate transient convection boundary condition associated with it. The wing was assumed to be totally isolated from the fuselage in this model, thus an adiabatic boundary condition was assumed at the fuselage. The internal surfaces of the wing were assumed to be diffuse-gray surfaces with an emissivity of 0.85. Results from the wing-box model showed that the convection boundary condition dominated the surface heating conditions such that external radiation and solar and earth IR heat fluxes had negligible effect, so they were not included in the full wing analysis. Natural convection inside the wing was also not considered.

Due to the large number of elements, and the problems encountered with view factor computations for such large models in the initial study, only the integration method was used to analyze the full wing model. The model consists of 235 elements and 725 nodes, and was analyzed using $p=2$, $p=3$, and $p=4$ elements. There are 725 degrees of freedom in the model using $p=2$ elements, 1769 degrees of freedom in the $p=3$ element model, and 3283 degrees of freedom in the $p=4$ element model. The model with $p=2$ elements was run with time steps of 0.1, 0.05, and 0.01 hours with no significant differences in the results. The $p=3$ and $p=4$ runs used a time step of 0.05 hours. All runs were

performed on a 200 MHz Pentium class personal computer.

A temperature contour plot of the upper surface of the wing at the beginning of the cruise portion of the trajectory (0.2 hours into the flight) is shown in Figure 14. First note that the temperature variation over the entire wing surface is not that large, 10 to 15 °F. Except for the outboard leading edge, the lowest temperatures on the wing occur near the fuselage where the wing is thickest. The deeper ribs and spars in this area act as heat sinks preventing the surrounding structure from heating as fast as other areas. Moving out from the fuselage (+y) the wing thins and the resulting internal structure becomes smaller. The smaller internal structure provides less thermal mass and the corresponding skin temperatures increase. Near the fuselage, the heat sink effect of the relatively massive internal structure can be clearly seen by the oval contours corresponding to individual wing-boxes. The oval contours occur because the temperature at the edges of the wing-boxes are held down by the adjacent internal structure while the temperatures at the center of the wing-box respond more rapidly. Figure 15 shows the corresponding temperature contours for the lower surface. Since the lower surface has a higher convection coefficient, it heats up faster than the upper surface. This is evidenced by the overall higher temperature in Figure 15 as compared to Figure 14. The temperature gradients on both surfaces disappear quickly, and are in fact gone by 0.3 hours as shown in Figure 16 and Figure 17.

To see the temperature response of the internal structure, the data for a spar, a rib, and a single wing-box have been extracted from the full wing data set. The approximate locations of the components are shown in Figure 17. Figure 18 shows the temperature contours for the selected rib at 0.2 hours. The same general patterns that were seen in the wing-box model appear here. The upper and lower surfaces of the spar are at uniform temperatures while the temperatures between the upper and lower surfaces are cooler. The lowest temperatures occur where the spars intersects the rib (vertical lines in Figure 18) halfway between the upper and lower surfaces. These patterns are also shown in Figure 19 where the temperatures along the upper and lower surface of the spar are plotted along with the temperature halfway between the upper and lower surfaces. The symbols on the line plot are used only to differentiate the curves, they do not represent the actual data points (each curve was generated using approximately 60 equally spaced temperature values). The mid-plane temperature profile shows a steep drop at the intersection of each spar. Figure 20 shows the

same temperature plots at 0.3 hours. The temperature variation along the mid-plane at this later time shows the same patterns that were present at 0.2 hours, although the overall temperature is higher and the magnitude of the variations has diminished. Figure 21 shows the results from the model with $p=4$ elements at 0.2 hours. The results are similar to the $p=2$ results with the $p=4$ elements producing a flatter temperature profile near the center of the wing-boxes.

The temperature contours for the selected spar at 0.2 hours using $p=2$ elements are shown in Figure 22. Once again the upper and lower surfaces are relatively warm with uniform temperatures. The lowest temperatures occur midway between the upper and lower surfaces where the ribs intersect the spar. As the wing thins moving out from the fuselage, the mid-plane temperatures (halfway between the upper and lower surfaces) increase and the gradients in the spar diminish. This pattern is also illustrated in Figure 23 where the temperatures along the upper, lower, and mid-plane surfaces for this spar at 0.2 hours are plotted. Figure 24 shows the same temperature plots at 0.3 hours. Once again, the overall structure temperature has increased and the magnitude of the temperature gradients have decreased relative to the earlier time point. Figure 25 shows the results from the model with $p=4$ elements at 0.2 hours. Again the results are similar to the $p=2$ results with the $p=4$ elements producing a flatter temperature profile near the center of the wing-boxes.

Finally, Figure 26 shows the temperature contours of the selected wing-box using the $p=2$ results at 0.3 hours. This wing-box is one of the larger wing-boxes in the wing and thus has some of the largest temperature gradients. The contours shown in Figure 26 have the same patterns as seen in the wing-box analysis. The coolest temperatures occur at the intersection of the ribs and spars halfway between the upper and lower surface. One slight difference is that the outboard rib is shorter than the inboard rib and results in lower gradients across the outboard section of the wing-box.

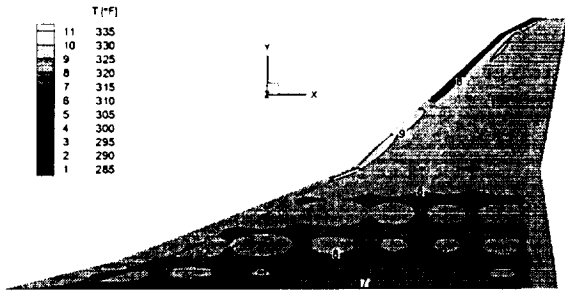


Figure 14: Temperature contours of the full wing model upper surface at 0.2 hours using p=2 elements.

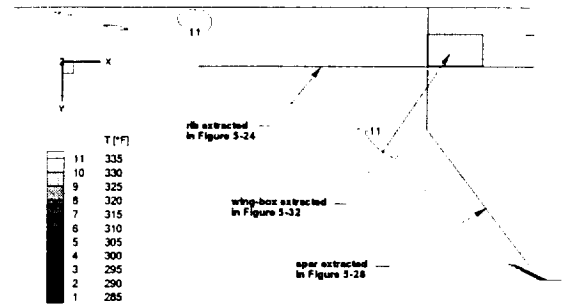


Figure 17: Temperature contours of the full wing model lower surface at 0.3 hours using p=2 elements.

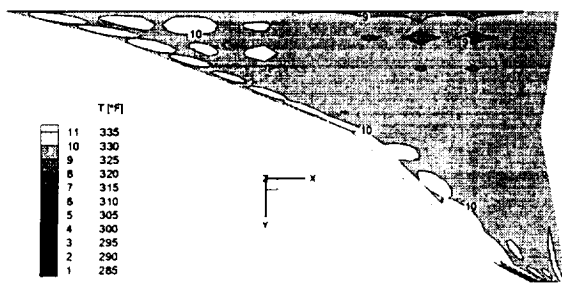
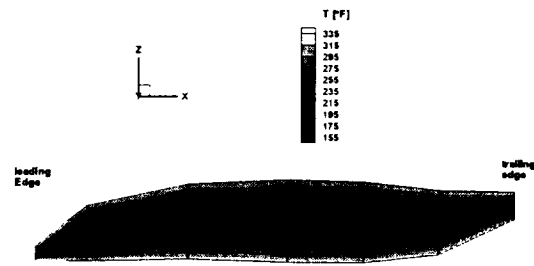


Figure 15: Temperature contours of the full wing model lower surface at 0.2 hours using p=2 elements.



Note: z dimension scale expanded to 5 times x dimension scale

Figure 18: Temperature contour for selected rib of full wing model at 0.2 hours using p=2 elements.

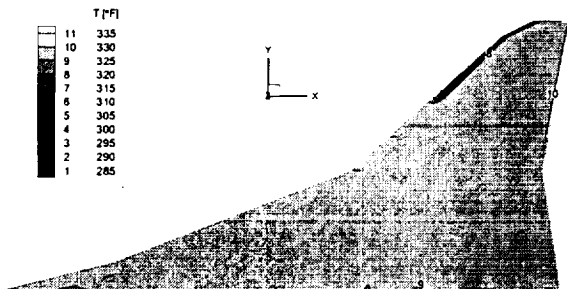


Figure 16: Temperature contours of the full wing model upper surface at 0.3 hours using p=2 elements.

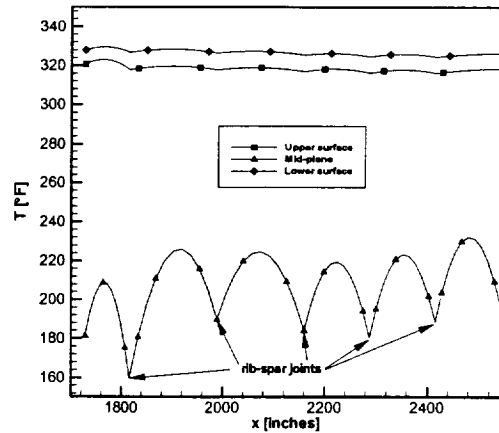


Figure 19: Temperatures along selected rib of full wing model at 0.2 hours using p=2 elements.

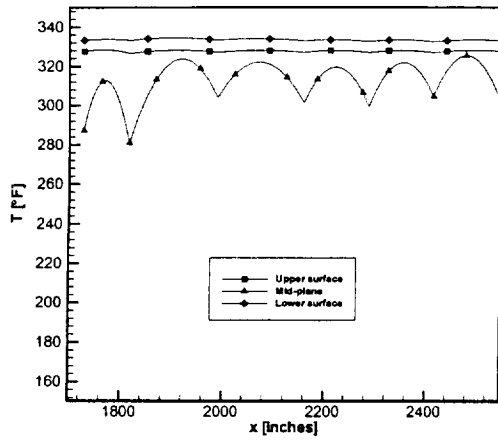


Figure 20: Temperatures along selected rib of full wing model at 0.3 hours using p=2 elements.

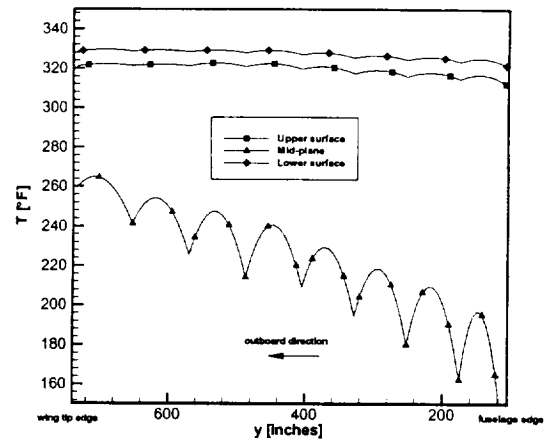


Figure 23: Temperatures along selected spar of full wing model at 0.2 hours using p=2 elements.

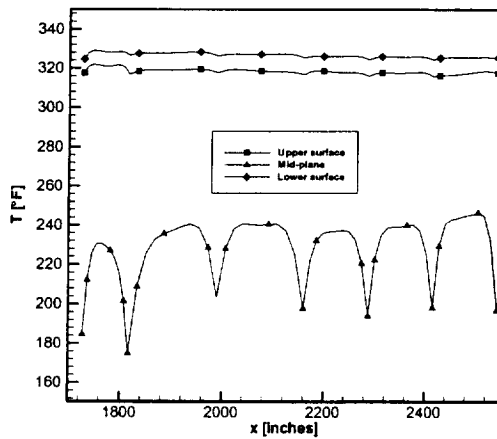


Figure 21: Temperatures along selected rib of full wing model at 0.2 hours using p=4 elements.

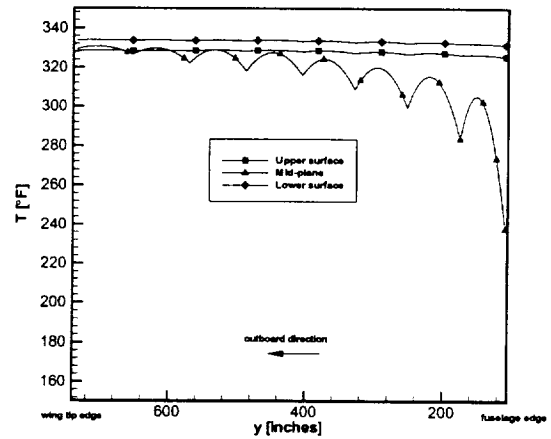
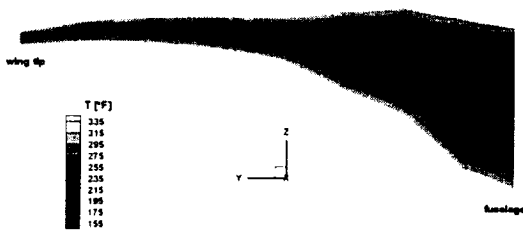


Figure 24: Temperatures along selected spar of full wing model at 0.3 hours using p=2 elements.



Note: z dimension scale expanded to 5 times x dimension scale

Figure 22: Temperature contour for selected spar of full wing model at 0.2 hours using p=2 elements.

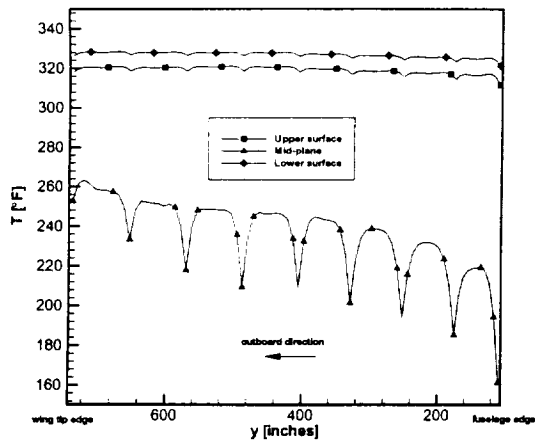


Figure 25: Temperatures along selected spar of full wing model at 0.2 hours using $p=4$ elements.

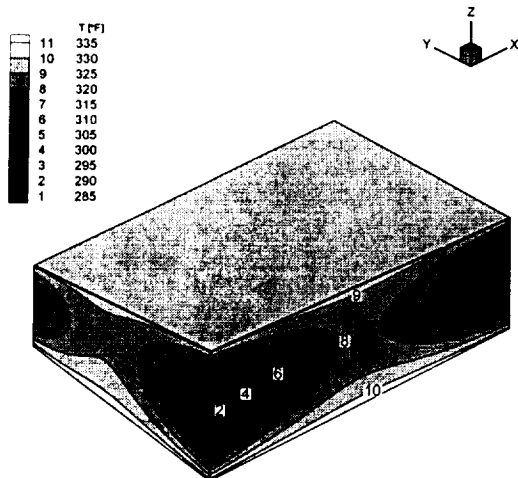


Figure 26: Typical wing-box extracted from full wing model, time = 0.3 hours, $p=2$ elements.

CONCLUSIONS

The methods developed in [1] have been used for the thermal analysis of a High Speed Civil Transport wing using a wing-box model as well as a full wing model. Results from the full wing model indicate that a solution with $p=2$ elements provides a good balance between accuracy and cost (execution time). The development of these methods was the result of an initial study that demonstrated the difficulties in analyzing a full wing model due to the complexities involved with the internal radiation heat exchange. The new methods provide a way to analyze the full wing structure accurately and efficiently. This capability is particularly useful in the conceptual design

stage of a vehicle when overall design parameters are of interest. The new methods will permit a better heat transfer representation of the internal structure and will thus give a more accurate prediction of the temperature distribution throughout the wing. The improved temperature distribution can then be used in a structural model of the wing to evaluate thermal stress. The refined temperature distribution will improve the thermal stress distribution producing a more accurate sizing of the structural components of the wing, an important factor since these vehicles are extremely weight critical.

- 1 Gould, D. C., "Radiation Heat Transfer Between Diffuse-Gray Surfaces Using Higher-Order Finite Elements", AIAA Paper 2000-2371, 2000.
- 2 Huebner, K. H., Thornton, E. A., Byrom, T. G., *The Finite Element Method For Engineers*, 3rd edition, John Wiley and Sons, New York, 1995.
- 3 Lobo, M., Emery, A. F., "The Discrete Maximum Principle I Finite-Element Thermal Radiation Analysis", *Numerical Heat Transfer*, Part B, Vol. 24, pp. 209-227, 1993.
- 4 Engel, C. D., Praharaj, S. C., *MINIVER Upgrade for The AVID System, Volume 1: LANMIN Users's Manual*, NASA CR-172212, 1983.